ELSEVIER

Biophysical Chemistry 75 (1998) 235–248

Biophysical Chemistry

A spectroscopic and molecular dynamics study of native and of a mutant of *Xenopus laevis* Cu,Zn superoxide dismutase: mechanistic consequences of replacing four charged amino acids on the 'electrostatic' loop

M. Falconi, F. Venerini, A. Desideri*

INFM and Department of Biology, University of Rome 'Tor Vergata', Via della Ricerca Scientifica, 00173 Rome, Italy

Received 20 July 1998; received in revised form 30 September 1998; accepted 30 September 1998

Abstract

Neutralisation by site-directed mutagenesis of four charged and highly conserved residues of the electrostatic loop of Cu,Zn superoxide dismutase from *Xenopus laevis*, involved in the electrostatic attraction of the substrate: Lys120 → Leu, Asp130 → Gln, Glu131 → Gln and Lys134 → Thr, gives rise to a mutant enzyme which displays an affinity for monovalent inhibitor anions, such as N_3^-, higher than that of the wild type. Analysis of 300 ps of molecular dynamics simulation carried out on the wild type and on the *Xenopus laevis* Cu,Zn superoxide dismutase mutant indicates that the two proteins display a distinct dynamical behaviour. In particular the root mean square deviation from the starting structure, the number of residues in random coil conformations, the number of residues in unfavourable regions of the Ramachandran plot indicate that the mutant displays a rigidity higher than the native enzyme. This is also evidenced by the loss of dynamical cross correlations in the simulation of the mutant, which on the other hand are present in the wild type. Moreover the mutant protein shows a different organisation of the backbone-to-backbone hydrogen bonds network that generates a rigid structure leading to an increase of the active site accessibility when compared to the native enzyme. It is suggested that the rigid state in which the mutant is confined, accompanied by the increase of the solvent accessible surface of the active site may explain the difference in reactivity toward the inhibitor anion.

Keywords: Molecular dynamics simulation; *Xenopus laevis* Cu,Zn superoxide dismutase; Site-directed mutagenesis; Structure–function relationship

* Corresponding author. Tel.: +39 6 72594376; fax: +39 6 72594326; e-mail: desideri@uniroma2.it

0301-4622/98/$ - see front matter
PII S0301-4622(98)00209-9

1. Introduction

Superoxide dismutases (Cu,Zn SODs) are a class of metallo-enzymes that catalyse the dismutation of superoxide into oxygen and hydrogen peroxide by alternate reduction and oxidation of a copper ion which constitutes the active redox center [1]. The folding of the dimer is globular and is constituted by two chemically equivalent subunits of 16 kDa (Fig. 1).

Cu,Zn SODs have been widely investigated both from a simulative and an experimental point of view [2–5]. The mechanism of attraction of the superoxide anion has been shown to be modulated by the electric field distribution of the amino acid residues surrounding the active site [6–10]. In this respect single or double neutralization of one of the four residues: Lys120, Lys134, Asp130, Glu131, have been found to play a major role in the substrate attraction toward the catalytic copper ion because of the perturbation of the electric field distribution around the protein [11–14], whilst Arg141, a residue fully conserved in the Cu,Zn SODs family, has been shown to play a determinant role either in the attraction or in the right orientation of the negatively charged substrate anion [15,16]. A recent study has shown that concomitant neutralization of the two positive (Lys120, Lys134) and the two negative (Asp130, Glu131) residues gives rise to a mutant (LQQT mutant) which, although having almost unaltered the electric field distribution around the protein, displays at low ionic strength an activity higher than that found in the native enzyme [17].

In order to shed light upon the reason of such increased catalytic rate we have carried out a spectroscopic investigation and a molecular dynamics (MD) simulation on the wild type and on the LQQT mutant. When compared to the native enzyme the mutant shows a higher affinity constant toward a competitive inhibitor anion such as azide. MD simulation indicates that the two proteins sample different configurational spaces and display different dynamical behaviour. These differences lead to structural changes of the mutant protein which may explain its different reaction properties toward the substrate and the anionic inhibitor.

2. Materials and methods

2.1. Preparation of mutants

Molecular mutant of the recombinant Cu,Zn superoxide dismutase from *X. laevis*, isoenzyme B (XSODB), was prepared in our laboratories by site-directed mutagenesis. In order to avoid possible contamination of bacterial Mn and Fe-SODs, wild type and mutant XSODs were constitutively

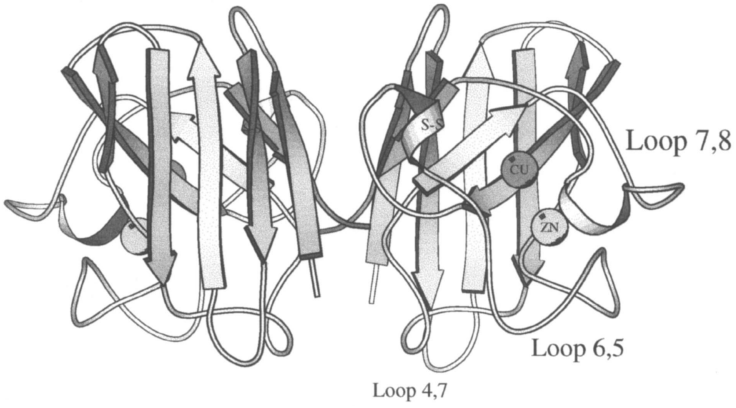

Fig. 1. Schematic view of the bovine Cu,Zn superoxide dismutase dimer. The arrows indicate the β-strands. The loops are represented as thin wires. The disulfide bridges are indicated by a label (S–S). The dark and light spheres represent the copper and the zinc ions, respectively. This picture was produced by using the MolScript 1.4 program [40].

produced in the *Escherichia coli* strain QC871 which is defective in the bacterial enzyme.

E. coli cells were disrupted as described by Marston [18]. Cell debris and insoluble proteins were removed by centrifugation and supernatants were subjected to $(NH_4)_2SO_4$ fractionation. Fractions containing XSODBs were pooled and purified to $> 98\%$ homogeneity, as judged by SDS-PAGE, by one or more steps on a Mono Q 5/5 FPLC column (Pharmacia).

2.2. Spectroscopic measurements

Absorption spectra of the protein were recorded at 20°C on a Lambda 9 Perkin Elmer spectrophotometer. Binding of N_3^- was monitored by following the intensity of the ligand to metal charge transfer band (LMCT) at 375 nm [19].

Each of the two isothermal curves has been fitted by the use of Eq. (1)

$$Y = 1/(1 + K/[N_3]_f) \quad (1)$$

where $[N_3]_f$ is the free azide concentration, Y is the molar fraction of the azide-bound enzyme and K is the binding constant for the N_3^-–SOD complex.

2.3. Molecular modelling

The mutant LQQT protein has been modelled by using the computer program Sybyl 6.0 by Tripos Associates. Residues were numbered according to the bovine sequence with no number for the Gly residue inserted (Gly after Glu25) and a number shift for the residue following the deleted residue Lys89 (Gly90 after Glu88).

The loop residues: Lys120, Asp130, Glu131 and Lys134 have been changed, respectively, into: Leu, Gln, Gln and Thr; conserving, when possible, the atomic positions of the sidechain atoms. After changing the sidechain atoms, these residues have been checked against contacts with the other residues. The sidechains of the substituted residues easily accommodate toward the solvent on the active site border.

2.4. Molecular dynamics

The molecular dynamics simulation has been performed using the computer program ORAC [20]. The coordinates of the *X. laevis* dimer at 1.49 Å resolution [21] were obtained from the Brookhaven Protein Data Bank (entry 1xso.pdb) [22]. The protein, in the X-ray configuration with its 353 crystal waters, has been inserted in the centre of a rectangular pre-equilibrated solvent box with volume of about $61 \times 85 \times 61$ Å^3 to give a water density of 1 g/cm^3 at 300 K. Solvent molecules that overlapped the solute or crystallographic water atoms by more than 10% were removed from the solvent box. With the remaining 8201 water molecules, the protein concentration was 5.25 mM. Six water molecules were replaced by sodium ions to make the system electroneutral. The water molecules were chosen far enough from each other and from the negative charges of the protein. During the simulation the sodium ions remain in the proximity of their starting positions surrounded by water molecules and do not enter in contact with the protein. The wild type system thus consisted of 27 239 atoms of which 2630 of the protein itself, 8201 water molecules and six sodium ions, while the mutant system consisted of 27 233 atoms of which 2624 of the protein itself, 8201 water molecules and six sodium ions. All polar hydrogen atoms have been included explicitly in the calculation, while those belonging to aliphatic and aromatic non-polar groups have been treated according to the united atom approximation [23]. Empirical simple point charge (SPC) model for water molecules [24] has been used in the simulation. For dynamics integration, the Verlet algorithm [25] with a time step of 2.0 fs has been used. All protein bond lengths were kept fixed by means of the SHAKE algorithm [26].

2.4.1. Potential function parametrization

The functional form of the potential employed is the same as for the CHARMM force field [23]. We used the united atom potential parameter set labelled CHARMM20. A group cutoff for elec-

trostatic interactions of solute and solvent was employed. A non-bonded interaction spherical cutoff of 10.0 Å, smoothed by a cubic spline between 9.0 Å and the cutoff distance, was used.

2.4.2. Thermalization and trajectory computations

Before starting the thermalization a preliminary energy-minimization of the proteins with their crystallographic water was obtained by using the conjugate gradient method implemented in the computer program MOIL [27]. The MD simulation was performed in the microcanonical ensemble (NVE). At the beginning of the simulation the kinetic energy was set at 300 K by initialising the atomic velocities with a Maxwell distribution. During equilibration the temperature was periodically scaled. The total potential energies of the two systems reach a plateau after about 40 ps. After the equilibration we ran the systems for a further 300 ps collecting distantly related protein coordinates once every 0.1 ps.

2.4.3. Dynamic cross-correlation map

The dynamic behaviours of these proteins in the MD simulation have been analyzed by using the dynamic cross-correlation map (DCCM) to yield information about possible correlated motions [28].

Correlated motions can occur among proximal residues composing the subdomain regions of Cu,Zn SOD subunit [29] but also between subdomains belonging to the same or to different subunits. The extent of correlated motions between residues is indicated by the magnitude of the corresponding correlation coefficient between their C_α atoms. The cross-correlation coefficient for the displacement of each pair of C_α atoms i and j is given by:

$$c_{ij} = \frac{\langle \Delta \mathbf{r}_i \cdot \Delta \mathbf{r}_j \rangle}{\sqrt{\langle \Delta r_i^2 \rangle \langle \Delta r_j^2 \rangle}} \qquad (2)$$

where Δr_i is the displacement from the mean position of the ith atom and the symbol $\langle\rangle$ represent the time average over the whole trajectory.

3. Results and discussion

3.1. Anion binding

The isothermal curve corresponding to the binding of the inhibitor anion azide to both the native and the mutant enzyme, worked out by the increase in absorbance at 375 nm, is reported in Fig. 2. Azide is known to bind directly to the catalytic copper atom giving rise to a new absorption band at 375 nm due to azide to copper charge transfer band [19] because of the azide binding to the equatorial plane of the copper coordination sphere [30]. This band in the wild type is characterised by an extinction coefficient ($\epsilon = 1350\ M^{-1}\ cm^{-1}$) higher than that of the mutant enzyme ($\epsilon = 1043\ M^{-1}\ cm^{-1}$), which may reflect a different overlap between the orbitals involved in the transition in the two enzymes.

The full lines reported in Fig. 2 represent the fit of the experimental data obtained through Eq. (1), reported in Section 2, from which an affinity constant of 143 ± 7 and $90 \pm 6\ M^{-1}$ for the mutant and for the native enzyme, respectively, is evaluated.

3.2. Molecular dynamics analysis

3.2.1. Overall properties

To assess the reliability of the calculations and as a measure of structural stability, we performed a series of standard tests on the geometrical properties of *X. laevis* wild type and mutant LQQT proteins. The stability checks were iteratively done running the DSSP program [31] which allows to measure during all the trajectory: the total number of hydrogen bonds, the number of residues in random coil conformation and the number of residues in unfavourable regions of the Ramachandran plot (i.e. with strained φ/ψ combinations) (see Fig. 3a–c).

In all cases the values of the structural parameters, chosen as a stability test, are fairly constant indicating a regular sampling around the equilibrium configuration of each protein. However the number of residues in random coil conformation

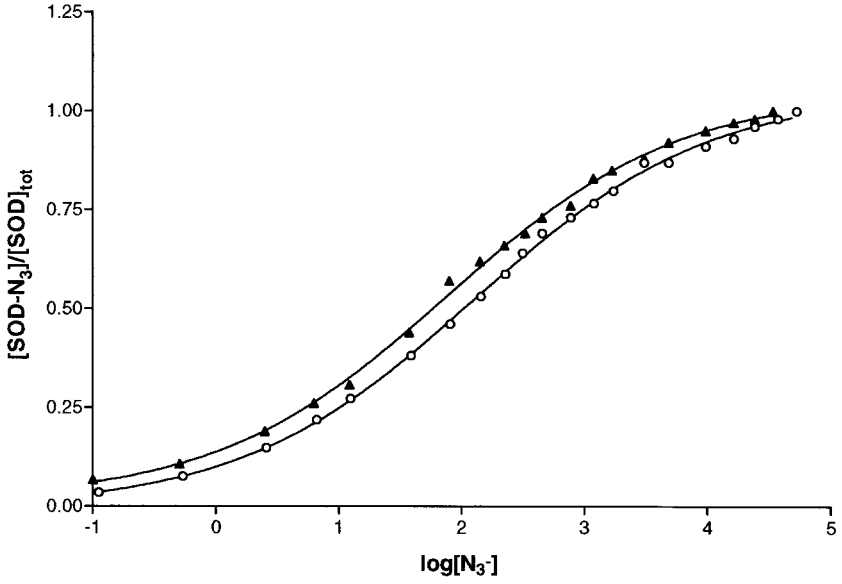

Fig. 2. Plot of the azide bound SOD fraction as a function of the logarithm of N_3^- concentration: wild type (○) and mutant (▲) protein. The titration was carried out at 20°C. The SOD was 2.0×10^{-4} M in 0.02 M phosphate buffer pH 7.4.

(Fig. 3b) and the number of residues in not allowed regions of the Ramachandran plot (Fig. 3c) is greater in the native than in the mutant enzyme over all the trajectory, while the opposite happens for the total number of intraprotein hydrogen bonds (Fig. 3a). This behaviour is consistent with a native structure sampling a conformational space larger than the mutant enzyme.

The all atom root mean square deviation (r.m.s.d.) from the starting equilibrated structure as a function of time was computed removing global translations and rotations and optimally superimposing the instantaneous configurations on the starting one and is reported in Fig. 3d for both the native and the mutant enzyme. In both cases the r.m.s.d. is lower than 3.0 Å indicating that the proteins are fluctuating around their starting configuration. However the phase-space accessibility sampled by the native enzyme is larger than that of the mutant protein, indicating that the wild type protein explores a number of conformations higher than the mutant during the trajectory.

Fig. 3e reports the plots of time evolution of the 'active sites surface' defined as the atoms enclosed in an 8.0 Å radius sphere from each copper atom. These spheres include the metals, the metal ligands and the fully conserved residue Arg141. The solvent accessible surface of the region surrounding and comprising the active copper is greater in the mutant than in the native enzyme during all the simulations length.

3.2.2. Hydrogen bonds analysis

In order to better relate the dynamical behaviour of the LQQT mutant with that of the wild type protein, the permanence time of intraprotein hydrogen bonds (H-bonds) were calculated for the two enzymes during all the simulation.

A geometric criterion was used to define the formation of an H-bond during the simulation: the hydrogen acceptor distance has to be shorter than 3.2 Å and the donor acceptor angle has to be larger than 120°. Only the H-bonds which are present in the simulation with a time percentage greater than 20% (60 over 300 ps) have been taken into consideration. They are 169 in the wild type and 172 in the mutant. Hydrogen bonds that are specifically present only in the wild type or mutant proteins have been termed 'unique' whilst bonds that are present in both proteins have been

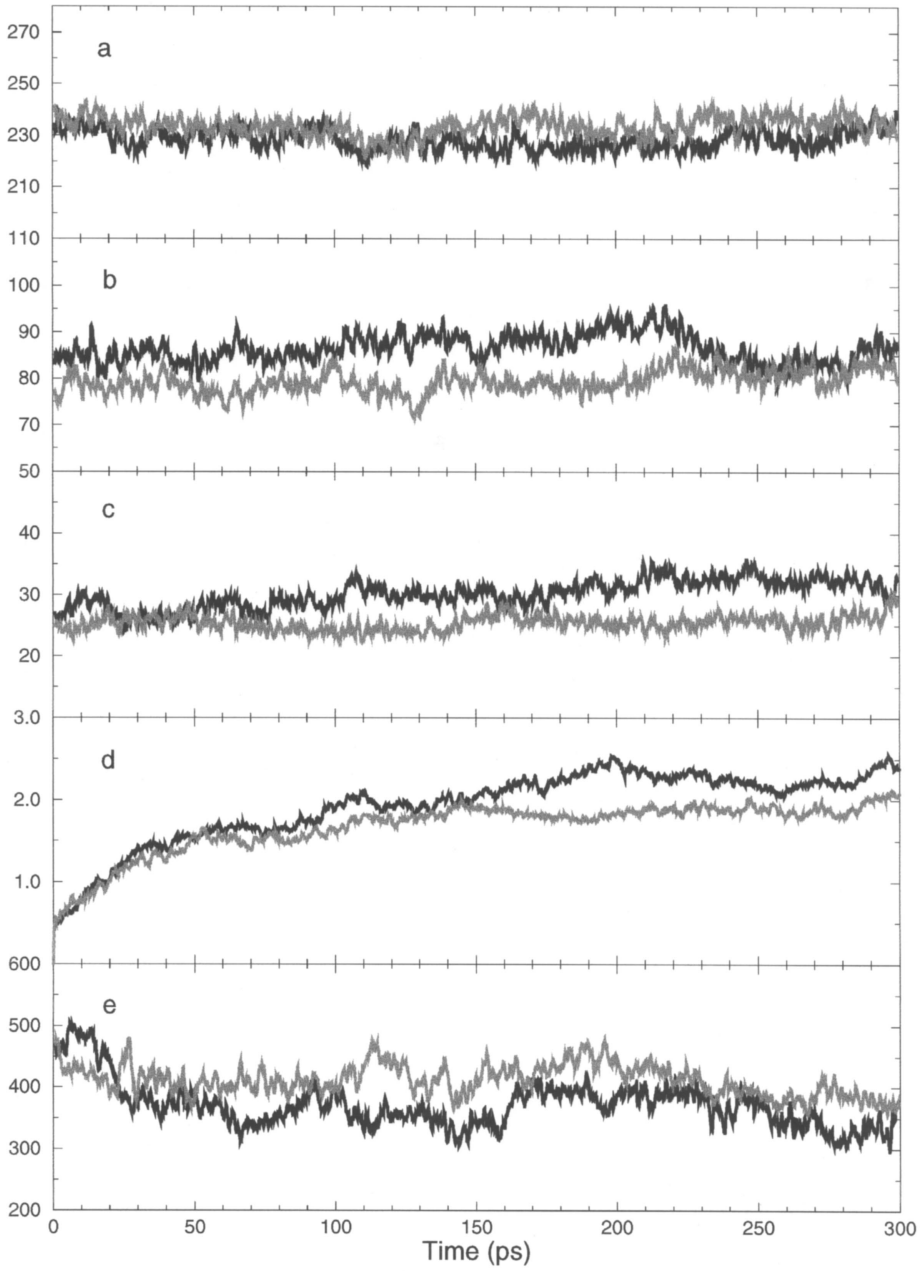

Fig. 3. Time evolution of geometrical properties of *X. laevis* wild type (——) and mutant (– – –) Cu,Zn SODs. (a) Total number of hydrogen bonds. (b) Number of residues in random coil conformation. (c) Number of residues in unfavourable regions of the Ramachandran plot. (d) All-atoms root mean square deviation from the thermalized starting structure. (e) Average solvent accessible active sites surface area ($Å^2$).

termed 'common'. It must be noted that for both the wild type and mutant proteins the H-bonds are not identical in the two subunits indicating the occurrence of dynamical asymmetry as already noticed by MD and X-ray diffraction studies [32–35]. In order to compare the different

flexibility of the native and mutant protein we considered the presence of the total number of H-bonds in the wild type and mutant protein without taking in consideration the difference in the two subunits.

We have first analyzed the 'common' hydrogen bonds dividing them in two groups.

- The first group is composed by H-bonds whose difference in permanence time between the mutant and the native protein is greater than 30%. To this group, represented by H-bonds which are more stable in the mutant than in the native protein, belong 17 H-bonds (see Table 1).
- The second group is composed by H-bonds whose difference in permanence time between the native and the mutant is greater than 30%. To this group which is represented by H-bonds which are more stable in the native than in the mutant protein, belong eight H-bonds (see Table 1).

Eight H-bonds in the wild type and 10 H-bonds in the mutant correspond to 'unique' H-bonds, i.e. they are present only in the native or in the mutant protein. Such a list is reported in Table 2. In the two proteins this class of H-bonds has the role to stabilize, although in different positions, the whole protein structure including the electrostatic loop 7,8 (the region in which the amino acid mutations were carried out).

In order to better visualize how the different location of the hydrogen bonds could change the fluctuation properties of the two proteins, they have been reported on a bidimensional picture of

Table 1
Backbone-to-backbone hydrogen bonds 'common' for both the wild type and the mutant SOD enzyme

H-bond			% of permanence in wild type	% of permanence in mutant
List of the backbone-to-backbone H-bonds having a permanence time greater in the wild type than in the mutant enzyme:				
ILE33/O	–	ALA93/N	87.20	35.63
GLY42/N	–	LYS-LEU120/O	81.70	36.27
PHE48/N	–	ALA58/O	78.50	41.10
GLY90/O	–	VAL92/N	85.13	22.87
ALA138/O	–	GLY140/N	72.60	25.23
LEU8/N	–	GLY16/O	96.50	53.10
HIS41/N	–	VAL85/O	84.40	34.90
PHE48/O	–	THR114/N	92.50	60.33
List of the backbone-to-backbone H-bonds having a permanence time greater in the mutant than in the wild type enzyme:				
VAL2/N	–	GLN22/O	45.87	92.83
VAL29/O	–	ILE97/N	24.23	57.33
GLY31/N	–	PHE95/O	27.70	65.60
GLY31/O	–	PHE95/N	24.00	87.30
PHE48/O	–	THR114/N	32.80	65.44
ASN129/O	–	LEU133/N	24.90	96.03
LEU8/O	–	GLY16/N	24.97	68.13
ASP24/O	–	GLY/N	24.07	59.23
VAL27/O	–	ASP99/N	56.80	90.17
GLY31/O	–	PHE95/N	40.73	83.07
ILE45/O	–	PHE62/N	44.43	94.10
GLY54/O	–	SER57/N	23.40	65.80
HIS69/N	–	LEU133/O	28.87	68.23
LEU124/O	–	LYS126/N	21.80	59.13
ASN137/O	–	GLY139/N	21.47	89.97
LYS-LEU120/N	–	ALA138/O	43.93	73.87
ASP-GLN130/O	–	LYS-THR134/N	23.40	86.27

Table 2
List of the 'unique' backbone-to-backbone hydrogen bonds

H-bond			% of permanence
Backbone-to-backbone H-bonds present only in the wildtype:			
ALA71/N	–	ASP76/O	51.27
ALA87/O	–	GLY91/N	32.83
SER11/O	–	VAL14/N	45.27
GLY70/O	–	HIS78/N	38.73
ALA71/O	–	HIS78/N	71.93
ALA87/O	–	GLY91/N	53.30
GLU131/O	–	LYS134/N	29.97
GLU131/O	–	THR135/N	94.60
Backbone-to-backbone H-bonds present only in the mutant:			
GLU88/N	–	GLN94/O	58.13
GLU88/O	–	GLN94/N	37.67
GLU119/N	–	GLY140/O	97.70
ASP123/O	–	GLY127/N	39.17
GLY42/N	–	LEU120/O	60.83
GLY49/O	–	ASN51/N	35.20
ASP50/O	–	THR52/N	34.40
GLU88/N	–	VAL92/O	77.43
GLU88/O	–	VAL92/N	72.56
ASP123/N	–	GLY136/O	37.70

the *X. laevis* structure in Fig. 4a,b for the wild type and the mutant enzyme, respectively. In Fig. 4a the 'common' H-bonds, whose difference in permanence time between the native and the mutant enzyme is greater than 30% (dashed line), plus the 'unique' H-bonds, which are present only in the native enzyme (full line), are reported. In Fig. 4b the 'common' H-bonds, whose difference in permanence time between the mutant and the native is greater than 30% (dashed line), plus the 'unique' H-bonds, which are present only in the mutant enzyme (full line), are reported.

Fig. 4a,b shows that, beside the fact that the number of H-bonds is higher in the mutant than in the wild type, the H-bonds have a very different distribution in the two proteins. In particular, in the wild type the H-bonds are spread over the global structure whilst in the mutant they are clustered between the β-strands, forming the β-barrel, and in the electrostatic loop 7,8, composing the active site region (see Fig. 4b). The different organisation of the hydrogen bond networks generates in the two proteins a dissimilar flexibility. In the mutant enzyme several sites of the backbone scaffold (i.e. β-strands 1a–2b, β-strands 3c–4f, N-terminal side of β-strand 4f with C-terminal side of β-strand 5e, middle part of β-strand 6d with C-terminal side of β-strand 7g and loop 7,8) are involved in forming stable H-bonds. The occurrence of such a H-bond network may explain the lower flexibility of the mutant enzyme already monitored through the parameters reported in Fig. 3. In particular, it may be guessed that the structural motions of the mutant protein are confined around specific positions and the enzyme may only explore a limited region of the phase-space while the wild type protein, being less constrained, is more flexible.

3.2.3. Amino acid fluctuation analysis

In order to verify if such difference in mobility spans over all the protein structure or is confined on some specific regions, atomic fluctuations ($\langle \Delta r_i^2/3 \rangle$) have been calculated and the difference between the native and the mutant enzyme, averaged over each amino acid and over the two subunits, have been reported in Fig. 5. The results indicate that the main difference is concentrated

in two regions corresponding to the loop 6,5 and 7,8 which accommodate the active site of SOD; in particular loop 6,5 provides the ligands to the zinc, whilst the electrostatic loop 7,8, where the four mutations have been carried out, shapes the channel which brings the substrate toward the catalytic copper ion. These two regions are extremely important since removal of the zinc is known to affect the Cu,Zn SOD structural stability [1] whilst the electrostatic loop 7,8 is directly

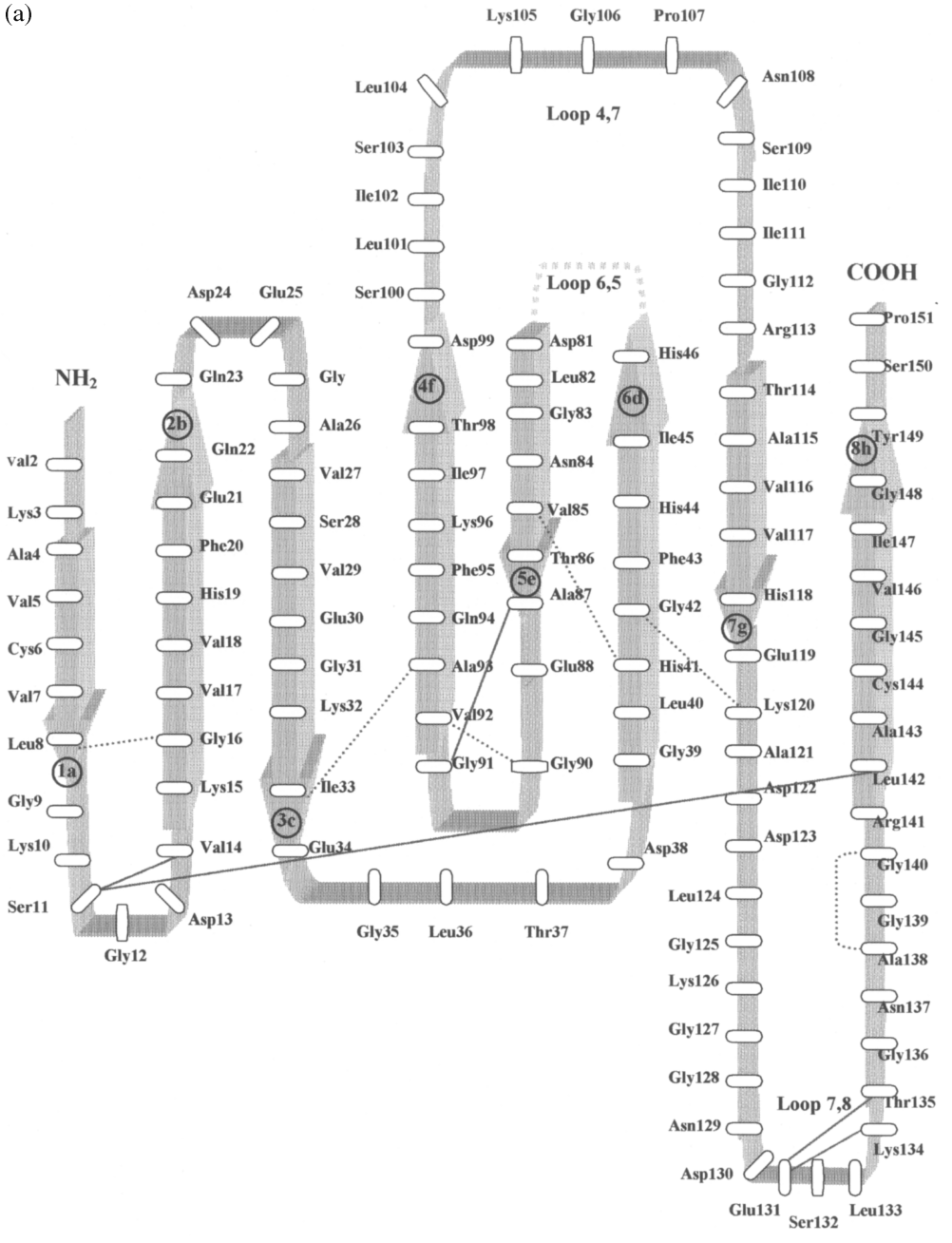

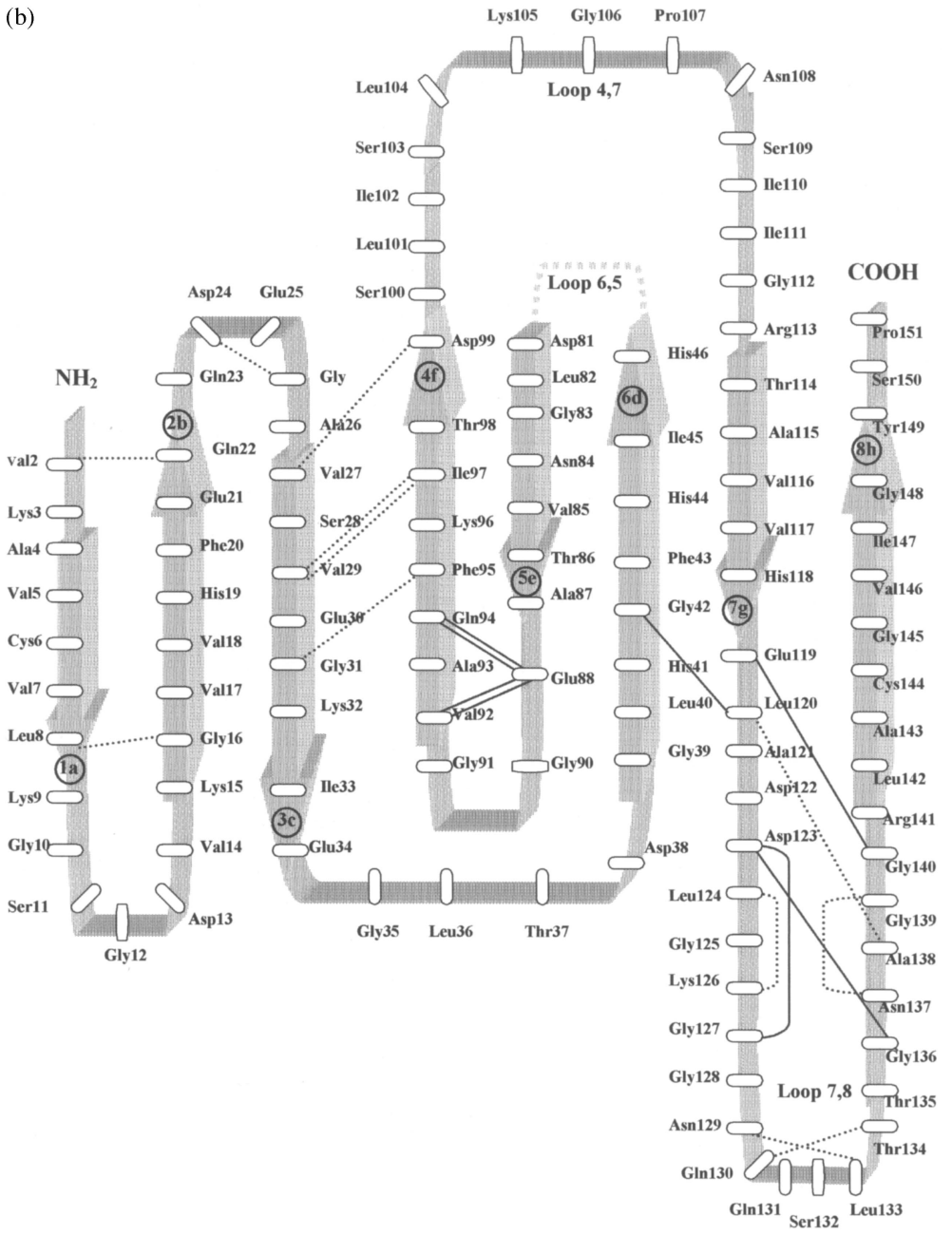

Fig. 4. (a and b) Schematic view of the topology of a *X. laevis* wild type (a) and mutant (b) Cu,Zn SOD subunit. The β-strands are represented by arrows, the loops and the turns by a continuous ribbon. The loop 6,5, too long to be displayed entirely in the figure, is represented by a dashed bold line. Backbone-to-backbone H-bonds are represented by dashed and full lines for the 'common' and 'unique' H-bonds, as defined in Tables 1 and 2, respectively.

connected to the attraction of the substrate [11–14].

3.2.4. Cross-correlation map analysis

Interesting results concerning the relative flex-

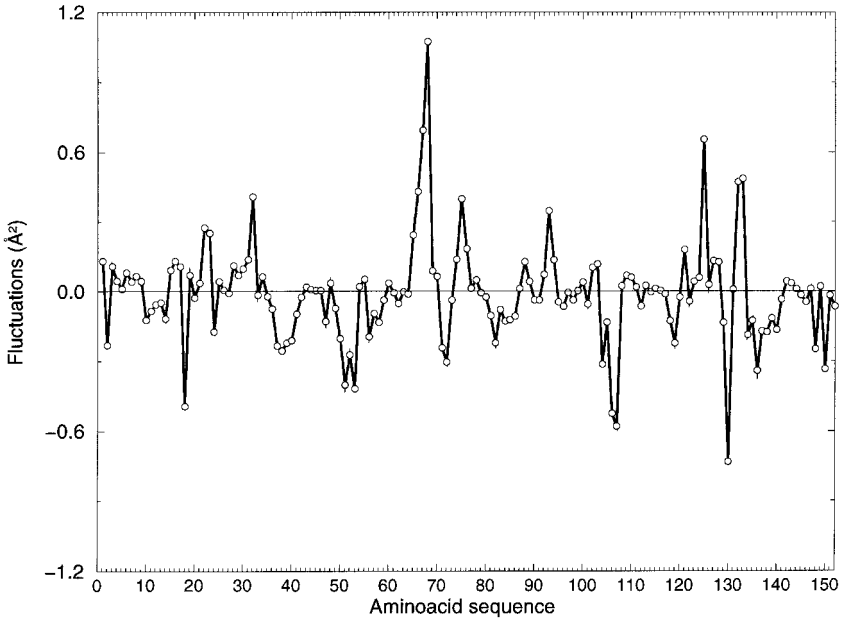

Fig. 5. Plot of the amino acid fluctuation difference between the native and the mutant enzyme. Values are averaged over the two subunits.

ibility and communication of the two enzymes may also be carried out by looking at the regions of the protein whose motion are correlated to the motion of other parts located in the same, or in the other subunit of the enzyme. In order to verify the existence of motion correlations between the sub-domains, belonging to the same subunit or to the different subunits, of the wild type and the mutant enzymes, the dynamic cross-correlation map defined in Section 2 [28] has been calculated.

Such plots are reported in Fig. 6a,b for the native and the mutant enzyme, respectively. In both cases the upper-left rectangle represents the intersubunit motion correlations while the lower-left and the upper-right triangles display the intrasubunit motion correlations for the A and B subunit, respectively. In both figures a black spot has been plotted only when the absolute value of the correlation between the two C_α is greater than 0.4, a threshold that has been used for other protein systems [36–38].

A striking feature immediately appears comparing the data of Fig. 6a,b, the native enzyme is characterised by a higher degree of intra and intersubunit correlation when compared to the mutant one. In particular, in the native enzyme, the Zn ligand region of loop 6,5 belonging to the active site of the first subunit is highly correlated with the electrostatic loop 7,8 belonging to the active site of the other subunit, as it has already been reported in the case of the bovine enzyme [32,33]. On the other hand the mutant enzyme, which is characterised by a higher rigidity, displays a lower degree of correlation in the motion of its two subunits that behave like almost independent units. It is interesting to note that although the four mutations are located in the proximity of the active site, far from the dimer interface, they are able to modify the mechanical communication between the two subunits indicating that amino acid composition of the active site may play a crucial role in tuning interaction and communication between the monomers.

4. Conclusions

Analysis of the molecular dynamics trajectories of the wild type and mutant proteins shows that the LQQT mutant is characterised by a higher

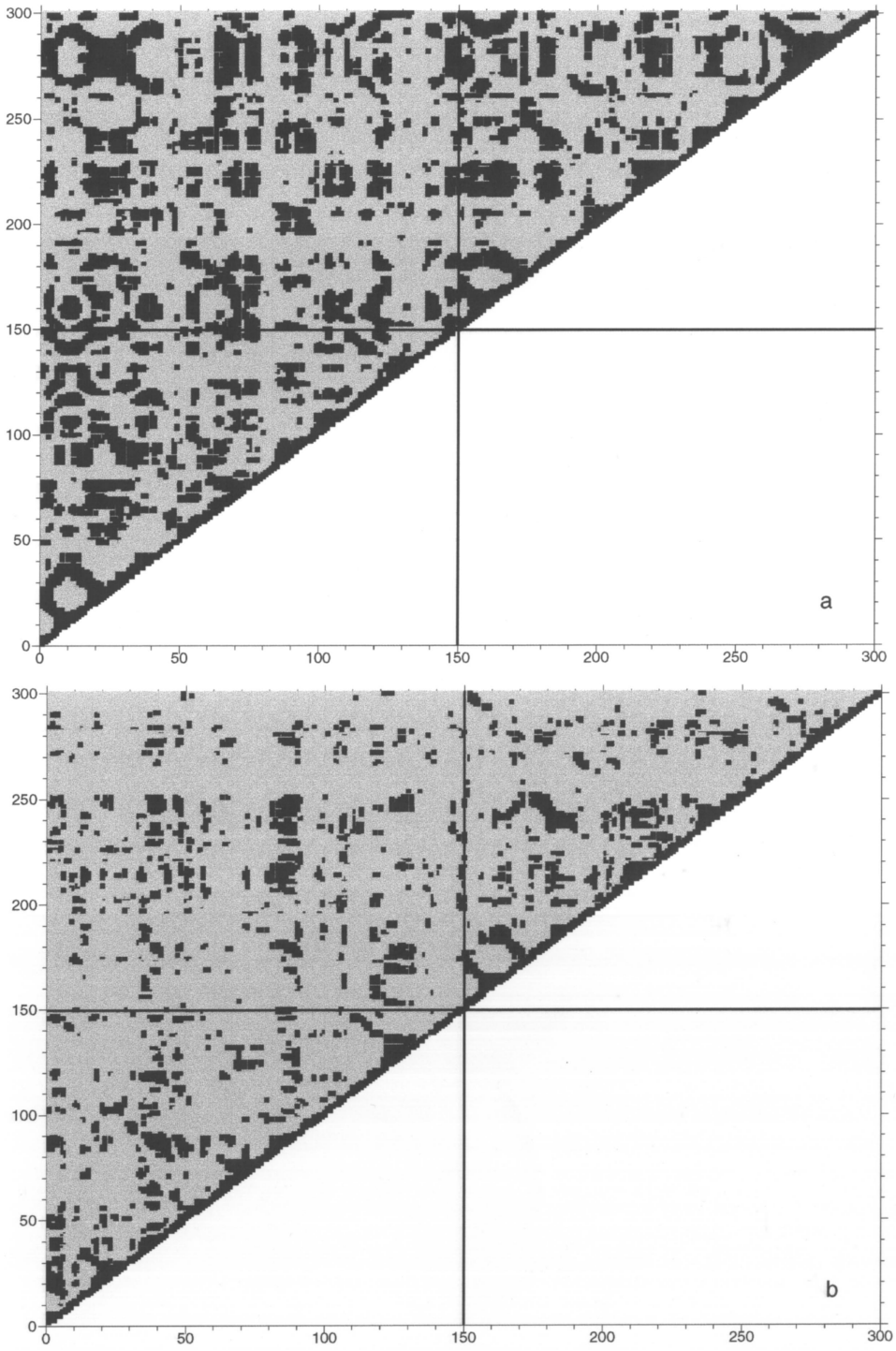

Fig. 6. (a and b) Dynamic cross-correlation map calculated for the wild type (a) and the mutant (b) Cu,Zn SOD dimers. The upper-left rectangle reports the intersubunit motion correlations, the lower-left and upper-right triangles the intrasubunit motion correlations for the A and B subunit, respectively. The black squares (■) represent $|c_{ij}| \geq 0.4$, while the grey squares (■) represent $|c_{ij}| < 0.4$ (c_{ij} is defined in Eq. (2) of Section 2).

degree of rigidity. Such a behaviour may be inferred by looking at Fig. 3b–d in which the number of residues in random coil conformations, the number of residues in not allowed regions of the Ramachandran plot as well as the r.m.s.d. from the starting equilibrated structure, respectively, are higher in the wild type than in the mutant protein. Moreover the total number of H-bonds is higher in the mutant than in the wild type protein (see Fig. 3a).

Analysis of Fig. 4a,b indicates that the rigidity of the LQQT scaffold is gained through a dynamical 'H-bonds cage' that limits the phase-space accessibility of the mutant protein fixing specific structural sites (Fig. 4b). In line, the number of H-bonds belonging to the 'common' group having a difference in permanence greater than 30% of total time, is more than two times higher for the mutant than for the wild type protein (17 vs. eight H-bonds, see Table 1). The presence of this 'H-bonds cage' also has the effect to impose specific constraints on the protein motion such as to block the occurrence of a mechanical communication between the two subunits, at variance with what is observed in the native enzyme. In fact Fig. 6a indicates that in the native enzyme the loop 6,5 of one subunit is strongly correlated with the electrostatic loop 7,8 of the other subunit, both loops being involved in defining the active site region of the enzyme.

Such an intersubunit correlation has been previously found in two independent MD simulations carried out in the bovine enzyme [32,33] suggesting the occurrence of a mechanical coupling between the two subunits. Such a correlation is almost absent in the mutant which displays a high degree of rigidity and as a consequence the two subunits have an almost independent behaviour. It is interesting to note that such a rigidity is coupled to an increased solvent accessible surface of the active sites which is higher in the mutant than in the native protein over all the trajectories (Fig. 3e).

The increase of surface area, representing the target of the substrate, may have a direct impact in the properties of this enzyme whose catalytic rate is limited by the diffusion [10–12]. In fact the second order catalytic rate (k_{cat}/k_M) is directly proportional to the second order association rate k_1 which depends on the probability of the substrate to enter the target area [10,11,39]. The increase of the solvent accessible surface area of the active site observed in the mutant is in line with its increased catalytic rate [17]. The increase of the solvent accessible surface area observed at the level of the active site may also explain the higher association constant displayed by the mutant for the inhibitory anion N_3^- (Fig. 2). However, such an effect is also an indication that the increase of the active site surface, beside providing a higher k_1 for the substrate, may also provide a higher target area for unspecific anions, thus explaining why evolution has not favoured such kinds of mutations.

Acknowledgements

We gratefully acknowledge Dr. Massimo Marchi for the use of his MD program ORAC. The authors are also grateful to Dr. Fabio Polticelli for helpful discussions.

References

[1] J.V. Bannister, W.H. Bannister, G. Rotilio, CRC Crit. Rev. Biochem. 22 (1987) 111.
[2] J. Shen, S. Subramaniam, C.F. Wong, J.A. McCammon, Biopolymers 28 (1989) 2085.
[3] J. Shen, J.A. McCammon, Chem. Phys. 158 (1991) 191.
[4] Y. Wong, T.W. Clark, J. Shen, J.A. McCammon, Mol. Simul. 10 (1993) 277–289.
[5] J.S. Valentine, M.W. Pantoliano, in: T.G. Spiro (Ed.), Copper Proteins, John Wiley, New York, 1981, p. 292.
[6] W.H. Koppenol, in: M.A.J. Rodgers, E.L. Powers (Eds.), Oxygen and Oxy-radicals in Chemistry and Biology, Academic Press, New York, 1981, p. 671.
[7] E.D. Getzoff, J.A. Tainer, P.K. Weiner, P.A. Kollman, J.S. Richardson, D.C. Richardson, Nature 306 (1983) 287.
[8] I. Klapper, R. Hagstrom, R. Fine, K. Sharp, B. Honig, Proteins 1 (1986) 47.
[9] A. Desideri, M. Falconi, F. Polticelli, M. Bolognesi, K. Djinovic, G. Rotilio, J. Mol. Biol. 223 (1992) 337.
[10] A. Sergi, M. Ferrario, F. Polticelli, P. O'Neill, A. Desideri, J. Phys. Chem. 98 (1994) 10554.
[11] J.J. Sines, S.A. Allison, J.A. McCammon, Biochemistry 29 (1990) 9403.
[12] E.D. Getzoff, D.E. Cabelli, C.L. Fisher, et al., Nature 358 (1992) 347.

[13] F. Polticelli, A. Battistoni, G. Bottaro, et al., FEBS Lett. 352 (1994) 76.
[14] F. Polticelli, G. Bottaro, A. Battistoni, et al., Biochemistry 34 (1995) 6043.
[15] C.L. Fisher, D.E. Cabelli, J.A. Tainer, R.A. Hallewell, E.D. Getzoff, Proteins 19 (1994) 24.
[16] M. Sette, M. Paci, A. Desideri, G. Rotilio, Biochemistry 31 (1992) 12410.
[17] F. Polticelli, A. Battistoni, P. O'Neill, G. Rotilio, A. Desideri, Protein Sci. (1998) in press.
[18] F.A.O. Marston, in: D.M. Glover (Ed.), DNA Cloning, A Practical Approach, IRL press, vol. III, 1987, p. 59.
[19] L. Morpurgo, C. Giovagnoli, G. Rotilio, Biochem. Biophys. Acta 322 (1973) 204.
[20] P. Procacci, T.A. Darden, E. Paci, M. Marchi, J. Comp. Chem. 18 (1997) 1848.
[21] K. Dijnovic-Carugo, A. Coda, A. Battistoni, et al., Acta Cryst. D52 (1996) 176.
[22] F. Bernstein, T. Koetzle, G. Williams, et al., J. Mol. Biol. 112 (1977) 535.
[23] B.R. Brooks, R.E. Bruccoleri, B.D. Olafson, D.J. States, S. Swaminathan, M. Karplus, J. Comp. Chem. 4 (1983) 187.
[24] H.J.C. Berendsen, J.P.M. Postma, W.F. Van Gunsteren, J. Hermans, in: B. Pullman (Ed.), Intermolecular Forces, Reidel, Dordrecht, 1981, p. 331.
[25] L. Verlet, Computer 'experiments' on classical fluids. Phys. Rev. 159 (1967) 98.
[26] J.P. Rickaert, G. Ciccotti, H.J.C. Berendsen, J. Comp. Phys. 23 (1977) 327.
[27] R. Elber, A. Roitberg, C. Simmerling, et al., Comp. Phys. Commun. 91 (1995) 159.
[28] J.A. McCammon, S.C. Harvey, Dynamics of Proteins and Nucleic Acids, Cambridge University Press, London, 1987, p. 66.
[29] E.D. Getzoff, R.A. Hallewell, J.A. Tainer, in: M. Inouye, R. Sarma (Eds.), Protein Engineering, Academic Press, New York, 1986, p. 41.
[30] K. Dijnovic-Carugo, F. Polticelli, A. Desideri, G. Rotilio, K.S. Wilson, M. Bolognesi, J. Mol. Biol. 240 (1994) 179.
[31] W. Kabsch, C. Sander, Biopolymers 22 (1983) 2577.
[32] M. Falconi, E. Paci, R. Gallimbeni, J. Comput-Aided Mol. Design 10 (1996) 490.
[33] G. Chillemi, M. Falconi, A. Amadei, G. Zimatore, A. Desideri, A. Di Nola, Biophys. J. 73 (1997) 1007.
[34] S. Melchionna, M. Falconi, A. Desideri, J. Chem. Phys. 108 (1998) 6033.
[35] P.J. Hart, L. Hongbin, M. Pellegrini, et al., Protein Sci. 7 (1998) 545.
[36] Y. Komeiji, M. Uebayasi, I. Yamato, Proteins 20 (1994) 248.
[37] W.E. Harte, S. Swaminathan, M.M. Mansuri, J.C. Martin, I.E. Rosemberg, D.L. Beveridge, Proc. Natl. Acad. Sci. USA 87 (1990) 8864.
[38] A. Ciocchetti, A.R. Bizzarri, S. Cannistraro, Biophys. Chem. 69 (1997) 185.
[39] G. Oshanin, A. Blumen, J. Chem. Phys. 108 (1998) 1140.
[40] P.J. Kraulis, J. Appl. Cryst. 24 (1991) 946–950.